2012

Predicting Delta Ferrite Content in Stainless Steel Castings

ISIJ International, Tokyo, v. 52, n. 6, supl., Part 1-2, pp. 1054-1065, MAR, 2012
http://www.producao.usp.br/handle/BDPI/36910

ISIJ International, Vol. 52 (2012), No. 6, pp. 1054–1065

Predicting Delta Ferrite Content in Stainless Steel Castings

Marcelo Aquino MARTORANO,[1)]* Caio Fazzioli TAVARES[2)] and Angelo Fernando PADILHA[1)]

1) University of São Paulo, Department of Metallurgical and Materials Engineering, Av. Prof. Mello Moraes, 2463, São Paulo, SP, CEP 05508-900 Brasil. E-mail: martoran@usp.br, padilha@usp.br
2) Açotécnica S.A., Via de Acesso João de Góes, 1900, Jandira, SP, CEP 06612-912 Brasil. E-mail: fazzioli@yahoo.com

(*Received on October 28, 2011; accepted on February 7, 2012*)

The distribution of delta ferrite fraction was measured with the magnetic method in specimens of different stainless steel compositions cast by the investment casting (lost wax) process. Ferrite fraction measurements published in the literature for stainless steel cast samples were added to the present work data, enabling an extensive analysis about practical methods to calculate delta ferrite fractions in stainless steel castings. Nineteen different versions of practical methods were formed using Schaeffler, DeLong, and Siewert diagrams and the nickel and chromium equivalent indexes suggested by several authors. These methods were evaluated by a detailed statistical analysis, showing that the Siewert diagram, including its equivalent indexes and iso-ferrite lines, gives the lowest relative errors between calculated and measured delta ferrite fractions. Although originally created for stainless steel welds, this diagram gives relative errors lower than those for the current ASTM standard method (800/A 800M-01), developed to predict ferrite fractions in stainless steel castings. Practical methods originated from a combination of different chromium/nickel equivalent indexes and the iso-ferrite lines from Schaeffler diagram give the lowest relative errors when compared with combinations using other iso-ferrite line diagrams. For the samples cast in the present work, an increase in cooling rate from 0.78 to 2.7 K/s caused a decrease in the delta ferrite fraction, but a statistical hypothesis test revealed that this effect is significant in only 50% of the samples that have ferrite in their microstructures.

KEY WORDS: stainless steel; casting; phase transformation; ferrite.

1. Introduction

Austenitic stainless steels have numerous applications due to a good combination of properties, such as, corrosion and oxidation resistance, toughness, weldability, and mechanical strength at low and high temperatures. Stainless steel properties and performance are strongly related to its microstructure, especially the amount and distribution of delta ferrite. In the case of castings and welds, these depend chiefly on chemical composition and on the cooling rate during and after solidification.[1)] Phase diagrams are important to predict the type and amount of phases present in stainless steel microstructures, but they are hardly available for steel compositions with more than five components, which is frequently the case in industrial applications. Therefore, practical methods based on empirical maps that indicate the amount and types of phases in the microstructure as a function of alloy chemical composition have been developed.[2)] Schaeffler[3)] was one of the first to propose an empirical diagram in which alloying elements were divided into two groups: austenite and ferrite stabilizers. Formulas were developed to calculate two indexes, namely a nickel equivalent (Ni_{eq}) and a chromium equivalent (Cr_{eq}), which quantified the effects of the austenite and ferrite stabilizers, respectively. General expressions for the Ni_{eq} and Cr_{eq} used by several authors are given below

$$Ni_{eq} = \%Ni + A_{Mn}\left(\%Mn\right) + B_C\left(\%C\right) + C_N\left(\%N\right) + D_{Cu}\left(\%Cu\right) + E_{Co}\left(\%Co\right) + F \quad \ldots (1)$$

$$Cr_{eq} = \%Cr + G_{Si}\left(\%Si\right) + H_{Mo}\left(\%Mo\right) + I_{Al}\left(\%Al\right) + J_{Nb}\left(\%Nb\right) + K_{Ti}\left(\%Ti\right) + L_W\left(\%W\right) + M_V\left(\%V\right) + N \quad \ldots (2)$$

where A_{Mn}, B_C, C_N, D_{Cu}, E_{Co}, F, G_{Si}, H_{Mo}, I_{Al}, J_{Nb}, K_{Ti}, L_W, M_V, N, are constant coefficients and the concentration of elements are in mass percent.

These indexes are represented as coordinates in the Schaeffler diagram, which is a two dimensional map of iso-ferrite lines, *i.e.*, contour lines of constant ferrite content. Although Schaeffler diagram was one of the first to be proposed, it is still used to predict the ferrite content in stainless steel welds.[4)] DeLong[5)] included the effect of N as an austenite stabilizer in the Ni_{eq} index and adjusted the inclination of some iso-ferrite lines of Schaeffler diagram, suggesting a new diagram for low ferrite contents ($\lesssim$14 mass%). Espy[6)] modified the Cr_{eq} and Ni_{eq} indexes after observing that the Schaeffler and DeLong indexes overestimated the effect of Mn and N in alloys with higher contents of these elements ($8 < \text{mass\%Mn} < 12.5$ and $0.14 < \text{mass\%N} < 0.31$). The effects of Cu, Al, and V were also included in these indexes. Siewert *et al.*[7)] analyzed more than 950 alloy compositions of stainless steel welds and suggested a new diagram and

new Cr_{eq} and Ni_{eq} indexes, in which only the effects of C, N, Mo, and Nb, besides Cr and Ni, were observed to be important. Later, Kotecki and Siewert[8] included a coefficient for Cu in the Ni_{eq} to improve the predictions of ferrite in stainless steel welds with higher Cu contents (> 0.3 mass%).

Although there are accurate studies about predicting ferrite contents in stainless steel welds using diagrams and equivalent indexes, little is available about the application of these practical methods to stainless steel castings. Schneider[9] developed a diagram and new Cr_{eq} and Ni_{eq} indexes including the effects of Co and V to predict the ferrite content in 12 mass% Cr heat-resistant steel castings. The proposed diagram seems to be a slight modification of the Schaeffler diagram, but nothing was mentioned about how it was obtained. Moreover, only the boundary lines with either a completely ferritic or completely austenitic structure were given (no other iso-ferrite lines were included). Guiraldenq[10] analyzed cast ingots (15 kg) made of typical 18-10 stainless steels and proposed a new coefficient for N in the Ni_{eq}, also including the effects of Al and Ti in the Cr_{eq}. Hull[11] examined thin castings and developed new Cr_{eq} and Ni_{eq} indexes. Hammar and Svensson[12] and the Jernkontoret[13] studied the solidification of stainless steels in controlled solidification conditions at cooling rates in the range between 0.1 and 2 K/s (typical of small and medium size castings), finally proposing new Cr_{eq}, and Ni_{eq}. None of these authors[10–13] suggested any diagram of iso-ferrite lines.

Schoefer[14] developed a complete method to predict the ferrite content in stainless steel castings by defining new Cr_{eq} and Ni_{eq} indexes and representing graphically the ferrite content as a function of the ratio between these equivalents. Neither the procedure used to obtain this diagram and the new expressions for the equivalent indexes nor the exact composition and number of alloys used in the analysis were reported. Later, this method was transformed into an ASTM standard,[15] without, again, any details about the development and accuracy of the method. For this method, the equation relating the ferrite percentage (*FE*) to the ratio between the equivalents (Cr_{eq}/Ni_{eq}) is given below[15]

$$\frac{Cr_{eq}}{Ni_{eq}} = 0.9 + 3.38883\cdot10^{-2}\,FE - 5.58175\cdot10^{-4}\,FE^2 + 4.22861\cdot10^{-6}\,FE^3 \quad \text{..... (3)}$$

The coefficients in Eqs (1). and (2) for the calculations of the Cr_{eq} and Ni_{eq} indexes proposed by several authors are summarized in **Table 1**. Although developed to predict the amount of delta ferrite content, these indexes have also been used to establish correlations among composition, properties and microstructures in stainless steel castings and cast samples.[16–18] Regardless of its application, a practical method and its equivalent indexes have been chosen from the methods discussed previously usually without any type of justification.

The objective of the present work is to examine the ability of the practical methods based on chromium (Cr_{eq}) and nickel (Ni_{eq}) equivalents and a diagram of iso-ferrite lines to predict the amount of delta ferrite in stainless steel castings. To investigate the predictability of these methods, sixteen specimens of five types of austenitic stainless steels were obtained by pouring the melt into an investment casting mold in which the average cooling rate during solidification was determined. In an attempt to increase the extent of the present analysis, the data published in the Jernkontoret report[13] and the results obtained by Hull[11] were also included in the analysis.

Table 1. Coefficients to calculate the Cr_{eq} and Ni_{eq} proposed by Schaeffler,[3] DeLong,[5] Schneider,[9] Guiraldenq,[10] Hull,[11] Schoefer,[14] Hammar and Svensson,[12] Espy,[6] and Siewert.[7]

	Scha 1949 Weld	DL 1960 Weld	Schn 1960 Cast	Guir 1967 Cast	Hull 1973 Cast	Scho 1977 Cast	H-S 1977 Cast	Esp 1982 Weld	Siew 1988 Weld
A_{Mn}	0.5	0.5	0.5	–	0.11	0.5	0.31	–	–
B_C	30	30	30	30	24.5	30	22	30[b]	35
C_N	–	30	–	20	18.4	26	14.2	30	20
D_{Cu}	–	–	–	–	0.44	–	–	0.33	–
E_{Co}	–	–	1	–	0.41	–	–	–	–
F	–	–	–	–	(a)	2.25	–	–0.48[b]	–
G_{Si}	1.5	1.5	2	1.5	0.48	1.5	–	1.5	–
H_{Mo}	1	1	1.5	2	1.21	1	1.37	1	1
I_{Al}	–	–	–	3	2.48	–	–	3	–
J_{Nb}	0.5	0.5	–	–	0.14	1	–	0.5	0.7
K_{Ti}	–	–	–	4	2.2	–	–	–	–
L_W	–	–	–	–	0.72	–	–	–	–
M_V	–	–	5	–	2.27	–	–	5	–
N	–	–	–	–	–	–4.99	–	–	–

(a) 0.0086 (mass% Mn)^2
(b) For $0 \le$ mass%N ≤ 0.2

2. Casting and Preparation of Samples

Stainless steel charges of approximately 100 kg were melted in a vacuum induction furnace and their chemical compositions (concentration of 16 elements) were measured by optical emission spectroscopy analysis of a small portion of the melt (**Table 2**). The stainless steel melt at the temperature indicated in Table 2 was poured into a ceramic mold made by the investment casting (lost wax) process. The mold had at least eight layers of a combination of colloidal silica slurry and zircon/alumina silicate stucco. After solidification and cooling to room temperature, specimens were extracted from the mold cavity. The specimen shape and dimensions are given in **Fig. 1**, showing different thicknesses in each step of a "ladder" to impose an increasing cooling rate from the thickest to the thinnest step. Three type R (Pt-13 mass%Rh, Pt) thermocouples were inserted into the mold cavity in contact with the metal to measure cooling curves at different positions. After combining these curves with simulation results from the software SolidCast®, the average cooling rates during solidification were estimated to be approximately 0.78, 0.75, 1.4, and 2.7 K/s for the ladder steps of thickenesses 40, 30, 20, and 10 mm, respectively.

The chemical composition was measured at three different locations of a ladder specimen obtained in one heat to verify the existence of any macroscopic variation in the concentration of elements (macrosegregation). Since these vari-

Table 2. Type of steel, chemical composition (mass%), and pouring temperature of the studied heats.

Steel	C	S	Mn	Si	Cr	Ni	Mo	P	Cu	Nb	N	Al	Ti	W	V	Co	Pouring T (°C)	Heat
AISI 302	0.22	0.009	1.05	1.05	17.4	11.4	2.34	0.043	0.13	0.69	0.0638	0.0014	0.0069	0.011	0.050	0.077	1 601	1
	0.21	0.009	0.891	1.06	17.4	11.0	2.05	0.003	0.11	0.57	0.0617	0.077	0.0073	0.01	0.044	0.096	1 515	2
	0.23	0.008	1.01	1.02	18.0	10.9	2.17	0.029	0.13	0.53	0.0576	0.0011	0.0078	0.01	0.049	0.087	1 532	3
AISI 304	0.043	0.004	1.09	0.776	18.4	9.37	0.322	0.039	0.17	0.0069	0.0580	0.0036	0.007	0.037	0.048	0.249	1 624	4
	0.038	0.005	0.563	0.399	17.9	10.7	0.110	0.020	0.048	0.0074	0.0270	0.001	0.0035	0.012	0.050	0.037	1 600	5
	0.085	0.009	0.677	0.801	18.7	9.25	0.314	0.030	0.12	0.017	0.0729	0.001	0.0034	0.015	0.048	0.083	1 529	6
	0.076	0.007	0.931	0.869	18.9	9.19	0.225	0.042	0.12	0.0064	0.0620	0.001	0.0044	0.017	0.047	0.083	1 608	7
	0.040	0.006	0.457	1.26	20.5	10.0	0.123	0.029	0.042	0.0072	0.0340	0.076	0.004	0.013	0.050	0.034	1 600	8
	0.033	0.007	0.415	1.34	19.5	10.0	0.116	0.027	0.042	0.007	0.0370	0.048	0.0034	0.014	0.049	0.036	1 600	9
	0.080	0.006	0.852	0.902	18.2	9.08	0.255	0.023	0.099	0.0062	0.0660	0.0017	0.0043	0.021	0.047	0.083	1 600	10
AISI 316	0.038	0.005	0.998	1.10	17.7	9.62	2.20	0.030	0.14	0.008	0.0476	0.0013	0.0048	0.012	0.048	0.086	1 600	11
DIN 1.4581	0.074	0.008	0.913	1.14	18.7	10.2	2.15	0.031	0.14	0.61	0.0571	0.0034	0.0064	0.013	0.051	0.075	1 633	12
	0.070	0.007	0.968	0.940	18.7	11.1	2.23	0.031	0.14	0.72	0.0568	0.001	0.0056	0.012	0.051	0.081	1 598	13
	0.065	0.008	0.713	0.985	18.5	10.5	2.19	0.029	0.14	0.49	0.0622	0.001	0.0061	0.013	0.053	0.076	1 600	14
	0.036	0.006	1.08	1.15	17.7	10.1	2.18	0.029	0.18	0.011	0.0340	0.0025	0.0078	0.017	0.050	0.091	1 600	15
DIN XG20	0.151	0.007	1.10	1.70	27.2	18.9	0.338	0.038	0.099	0.016	0.0523	0.002	0.0071	0.012	0.078	0.072	1 628	16

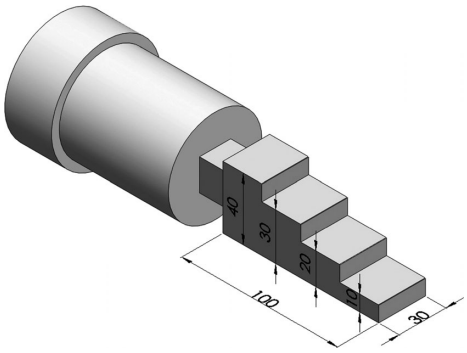

Fig. 1. Test specimen geometry ("ladder") showing four different thicknesses (10, 20, 30, and 40 mm) and the feeder (cylinder on the left) used to prevent shrinkage defects. Dimensions are in mm.

ations were within the experimental error of the analytical technique, macrosegregation of elements was not significant.

The delta ferrite content was determined with a Fischer feritscope model MP30E at several locations on a longitudinal section of the ladder specimens, yielding a complete delta ferrite distribution. The delta ferrite morphologies were observed by optical metallography after preparation of samples by grinding, mechanical polishing with diamond paste, and finally etching with aqua regia (100 ml HCl + 3 ml HNO_3 + 100 ml methyl alcohol).

3. Measurements of Delta Ferrite Content

The delta ferrite fractions measured in the present work samples were in the range of 0 to 12 vol% (**Table 3**). **Figure 2** shows two typical maps of delta ferrite, measured on the samples of heats 4 and 9. The average and standard deviation of the ferrite fraction measurements were calculated for each step of the ladder and for the whole sample, as shown in Table 3. In the next sections, the effects of cooling rate on the amount of delta ferrite is analyzed by comparing average ferrite fractions from different ladder steps, whereas

Table 3. Delta ferrite fraction (vol%) measured with the feritscope: average fractions and standard deviations are given for each ladder step thickness and for the whole sample (Global). The range of the number of ferrite measurements carried out in each ladder step and in the whole sample is indicated as N.

Heat	Thickness (mm)				Global N = 86–100
	10 N = 32–40	20 N = 24–30	30 N = 20	40 N = 10	
1	0	0	0	0	0
2	0	0	0	0	0
3	0	0	0	0	0
4	4.2±0.3	4±1	5±1	4.6±0.7	4.5±0.9
5	1.8±0.4	1.8±0.5	1.8±0.7	1.5±0.6	1.7±0.6
6	1.5±0.3	1.8±0.5	2.2±0.6	2.4±0.9	2.1±0.7
7	2.8±0.3	3.0±0.8	3.4±0.9	3.1±0.9	3.1±0.9
8	10.6±0.6	11±1	12±1	11±2	11±1
9	6.5±0.4	7.2±0.6	7.5±0.9	8±1	7.5±0.9
10	1.8±0.6	1.7±0.8	1.8±0.8	1.7±0.6	1.8±0.7
11	8.1±0.5	8.8±0.7	10±1	10±1	10±1
12	7.1±0.4	8.1±0.5	8.1±0.9	8.3±0.9	8.1±0.9
13	4±1	4.7±0.8	5.0±0.8	5.3±0.7	4.9±0.9
14	6.2±0.7	7.1±0.9	7±1	6±2	7±2
15	8.1±0.6	8.8±0.6	10±1	10±1	10±1
16	0	0	0	0	0

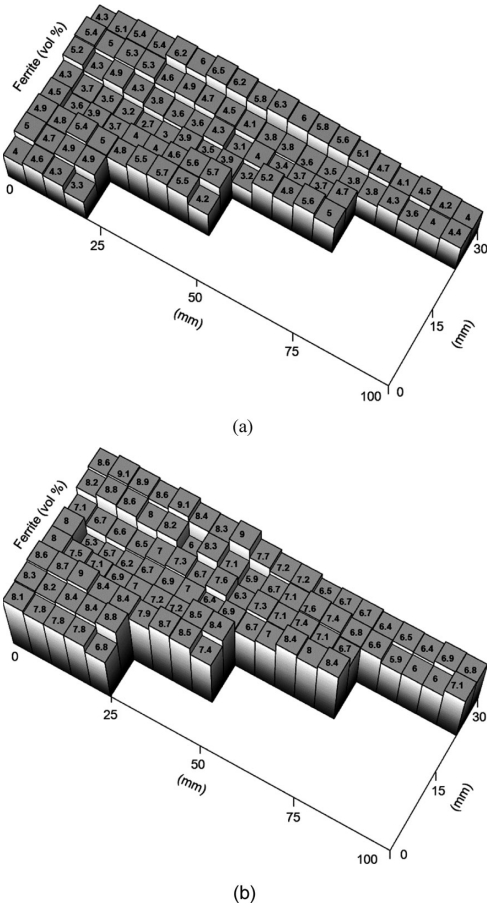

Fig. 2. Delta ferrite measurements on a longitudinal section across the center of the ladder specimens obtained in (a) heat 4 and (b) heat 9.

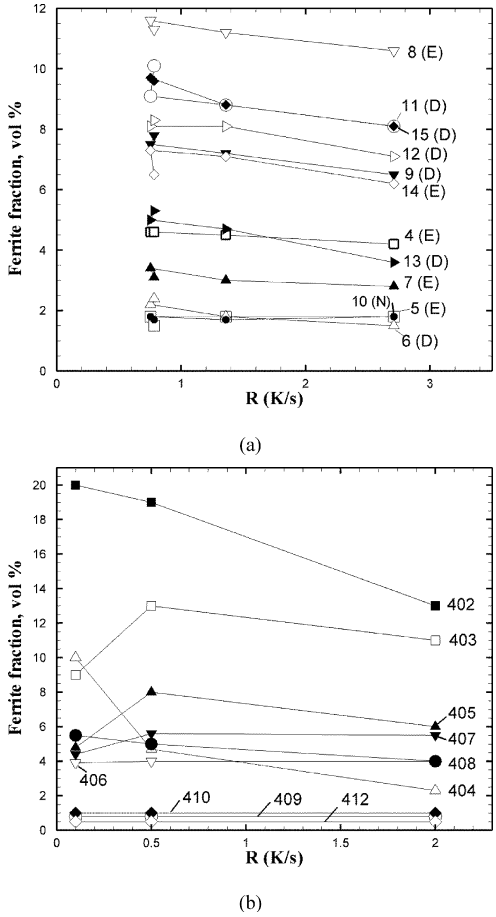

Fig. 3. Measured delta ferrite fraction (vol%) as a function of cooling rate during solidification (R): (a) for the present work samples in the heats indicated by the number on the right of each curve and (b) for the samples given in the Jernkontoret report,[13] also identified by a number on the right. For the present work samples in (a), also shown is the result of a hypothesis test to verify whether the average ferrite fractions in the thickest and thinnest steps of the same specimen are equal (E), *i.e.*, the null hypothesis, or different (D), with a 5% significance level.

the effects of composition is examined by comparing the global averages from different samples, *i.e.*, different heats.

4. Effect of Cooling Rate on the Amount of Delta Ferrite

The effect of cooling rate on the amount of delta ferrite is shown for each specimen in **Fig. 3**(a). Each measured point corresponds to the average fraction in one ladder step (Table 3), with which an average cooling rate during solidification is associated. A simple analysis of the average values shows a tendency of decreasing ferrite content with increasing cooling rate. As can be seen in Fig. 2, however, the amount of delta ferrite fluctuates within each step. To consider these fluctuations in the analysis of the cooling rate effect, a hypothesis test was carried out by comparing the averages of ferrite content between the thinnest (10 mm) and the thickest (40 mm) steps, for which the cooling rates were 2.7 and 0.78 K/s, respectively. In this analysis, the effects of fluctuations were readily taken into account in the variance of delta ferrite measurements within one ladder step. The null hypothesis of the analysis, defined as the equality between the averages (E), was accepted when[19]

$$\frac{|FE_1 - FE_2|}{S\sqrt{\frac{1}{N_1}+\frac{1}{N_2}}} < t_{\alpha,N_1+N_2-2} \quad \text{..... (4)}$$

where

$$S^2 = \frac{(N_1-1)S_1^2 + (N_2-1)S_2^2}{N_1+N_2-2} \quad \text{..... (5)}$$

FE_1 and FE_2 are the average ferrite contents in the two ladder steps; S_1^2 and S_2^2 are the associated sample variances (a sample is the set of measurements within either the thickest or the thinnest step); N_1 and N_2 are the number of measurements within each ladder step; and t_{α,N_1+N_2-2} is the value of the t-Student distribution for a significance level of 5% ($\alpha = 0.05$) with $N_1 + N_2 - 2$ degrees of freedom. When Eq. (4) is not fulfilled, the alternative hypothesis, *i.e.*, that the average ferrite contents in the steps are different (D) is accepted, indicating a significant cooling rate effect.

In Fig. 3(a) the results of the hypothesis tests are indicated on the right of each curve. In five specimens, the averages are equal, *i.e.*, there is no effect of the cooling rate, while in six specimens an increase in cooling rate decreases the amount of delta ferrite. Therefore, the cooling rate seems to have a weak effect of decreasing the amount of delta ferrite in these cast samples in the cooling rates from 0.78 to 2.7 K/s. In agreement with the present work, the Jernkontoret[13]

showed a negligible effect of the cooling rate during solidification (in the range between 0.1 and 2 K/s) on the amount of delta ferrite measured just below the solidus temperature. On cooling to room temperature, the ferrite content changed to a final fraction presented in Fig. 3(b). The authors[13] did not discuss the effects of cooling rate on this delta ferrite fraction (measured after cooling to room temperature), but the results given in Fig. 3(b) do not show any clear tendency, confirming the weak effect of the cooling rate.

To further examine the effect of the cooling rate, the microstructure and the solidification mode of the present work samples were investigated. In the metallographic analysis, the only sample with more than 10 vol% ferrite showed an almost continuous ferrite network microstructure (**Figs. 4**(a) and 4(b)), which deteriorates toughness owing to ferrite embrittlement by high temperature exposition.[20] In the samples with delta ferrite fractions of about 5 vol% (Figs. 4(c) and 4(d)), the ferrite network was semi-continuous, while for lower fractions (~ 2 vol%) the ferrite was arranged in isolated cores (Figs. 4(e) and 4(f)). Although the cooling rate seems to have a weak effect on the amount and morphology of delta ferrite, the size of the dendritic structure is significantly affected by a change in cooling rate from 0.78 K/s to 2.7 K/s. This effect can be seen by comparing Figs. 4(a), 4(c), and 4(e), which are from samples of the thickest step (0.78 K/s), with Figs. 4(b), 4(d), and 4(f), which are from samples of the thinnest step (2.7 K/s).

El Nayal and Beech[21] and Suutala and Moisio[22] defined a criterion based on the ratio of Cr_{eq}/Ni_{eq} proposed by Hammar and Svensson[12] to determine which of the following solid-

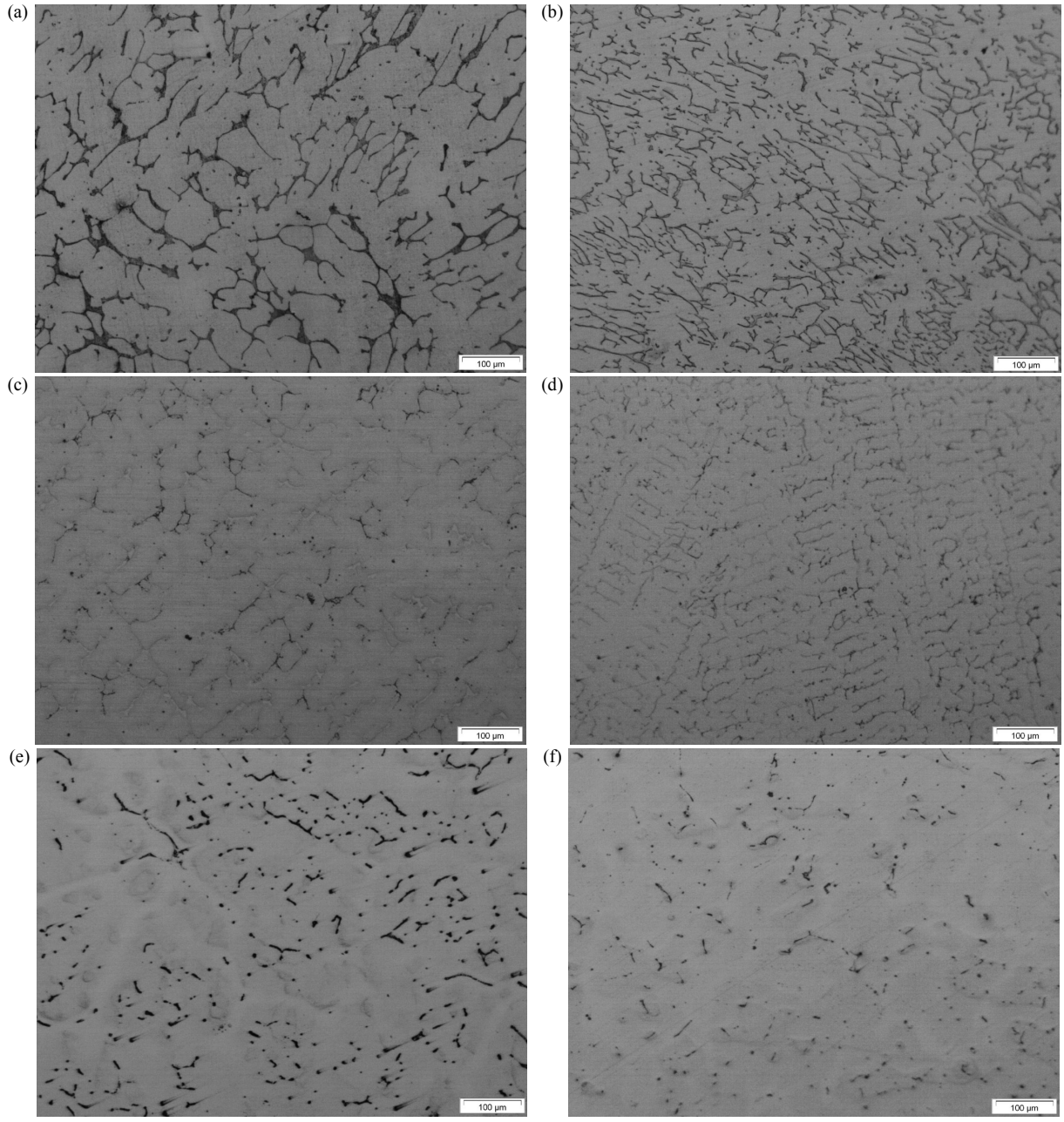

Fig. 4. Types of delta ferrite structure (in austenitic matrix) observed in the present work samples by optical microscopy. Delta ferrite is continuous in (a) and (b) (heat 8), semi-continuous in (c) and (d) (heat 13), or present in isolated cores in (e) and (f) (heat 6). The cooling rate is 0.78 K/s in (a), (c), and (e), and is 2.7 K/s in (b), (d), and (f).

ification modes is observed in austenitic stainless steels: mode A (L→L + γ→γ), mode AF (L→L + γ→ L + γ+ δ →γ+ δ), or mode FA (L→L + δ→ L + δ+ γ→γ+ δ). In this sequence, L is the liquid phase, γ is austenite and δ is ferrite. According to this criterion, heats 1, 2, 3, and 16 solidified in mode A; therefore, the related microstructures did not have any ferrite. On the other hand, samples from heats 4 to 15, which showed some delta ferrite in the microstructure, solidified in mode FA, *i.e.*, with ferrite as the leading phase and formation of interdendritic austenite at the expense of ferrite dendrites during solidification. After solidification, during cooling to room temperature, further austenite might form, consuming ferrite. In the FA mode, the change from ferrite to austenite depends on the diffusion of solute elements in the solid phases.

For samples solidifying in mode FA, Pereira and Beech[23] showed that no ferrite would be present at room temperature if equilibrium conditions prevailed. Consequently, the existence of ferrite at room temperature is an indication of limited solute diffusion caused by relatively large cooling rates. An increase in cooling rate both during and after solidification (on cooling to room temperature) should increase the amount of ferrite at room temperature, as observed by Elmer[24] and Pereira and Beech.[23] Nevertheless, Pereira and Beech,[23] and Kim *et al.*[25] observed that, in relatively large ingots and plates, in which the cooling rates change significantly along the ingot cross section, there is a decrease in ferrite content towards the ingot surface, where the largest cooling rate exists. Kim *et al.*[25] investigated this behavior in detail and showed that the importance of diffusion in promoting the $\delta \rightarrow \gamma$ transformation actually depends on both $\sqrt{Dt}$ and λ, where D is the solute diffusion coefficient in the solid, t is the time available for diffusion (during and after solidification), and λ is the spacing between secondary dendrite arms. Brody and Flemings,[26] and Flemings[27] showed that solid diffusion is more pronounced for larger $Fo = \sqrt{Dt}/\lambda$ values, where Fo is the mass diffusion Fourier number. As briefly explained in the Jernkontoret[13] report, the faster cooling rate at the ingot surface, compared with its center, produces a fine dendritic structure that can be more rapidly homogenized on cooling below the solidus. This more important role of diffusion at the surface rather than at the center of ingots has also been verified in studies of microsegregation.[28]

As discussed about the present work samples, a weak trend of a decreasing amount of delta ferrite with an increasing cooling rate is observed (Fig. 3(a)). To further investigate this behavior, an analysis similar to the one presented by Kim *et al.*[25] was carried in the present samples to quantify the role of Cr and Ni diffusion in the dissolution of ferrite during the peritectic and solid state transformations. The Fourier number for the peritectic, Fo_p, and solid-state transformations, Fo_s, were calculated for Cr and Ni in the thinnest and thickest steps of the ladder samples for the steels obtained in heats 8 and 13, described in Table 2. For this analysis, presented in **Table 4**: (a) the spacing between secondary dendrite arms, λ, was measured in the ladder steps; (b) the corresponding peritectic time, t_p, was estimated dividing the temperature interval between the peritectic and solidus temperatures by the measured cooling rate, R; and (c) the time for diffusion during solid-state transformation, t_s, was also estimated by dividing the temperature interval for solid-state transformation by the same measured cooling rate. The steel of heat 8 is a typical AISI304, which was also studied by Kim *et al.*[25] Therefore, some parameters adopted by these authors were also used in the calculations as follows: the peritectic temperature interval (36°C), the solid-state transformation interval (221°C), and the average temperature for the peritectic (1 410°C) and solid-state (1 300°C) transformations to calculate the diffusion coefficients using the equations given by Kim *et al.*[25] The steel in heat 13 is a DIN 1.4581, which is similar to the AISI 316 Nb studied in the Jernkontoret[13] report, from which the following estimates were obtained: peritectic temperature interval (135°C), solid-state transformation interval (115°C), average peritectic temperature (1 342°C) and average solid-state temperature (1 218°C) to calculate the diffusion coefficients.

Table 4. Analysis of the importance of diffusion of Cr and Ni in delta ferrite dissolution. For heats 8 and 13, the ladder step thickness (L), spacing between secondary dendrite arms (λ), cooling rate (R), peritectic time (t_p), time for solid-state dissolution (t_s), Fourier number for peritectic (Fo_p) and solid state dissolution (Fo_s) for Cr and Ni are shown.

Heat	L (mm)	λ (μm)	R (K/s)	t_p (s)	t_s (s)	Fo_p (Cr)	Fo_s (Cr)	Fo_p (Ni)	Fo_s (Ni)
8	10	11.1	2.7	13	82	0.15	0.20	0.12	0.16
8	40	28.9	0.78	46	283	0.10	0.14	0.08	0.11
13	10	17.7	2.7	50	43	0.12	0.05	0.10	0.04
13	40	39.4	0.78	173	147	0.10	0.04	0.08	0.03

Finally, Fo_p and Fo_s were calculated and presented in Table 4, showing that Fo in the thinnest step is larger than that in the thickest step for both Cr and Ni in the two types of steel. This indicates that the diffusion processes occurring in the thinnest step are more intense, which implies that the dissolution of ferrite, which is dominated by diffusion of solute elements, should occur to a larger extent, resulting in a lower ferrite content at the thinnest step as observed in Fig. 3(a). To conclude, in the ladder samples an effect of diffusion similar to that observed in relatively large ingots occurred, *i.e.*, an increase in $\sqrt{Dt}/\lambda$ from the thickest to the thinnest step. Since the steps are connected to each other, the thinnest step seems to play the role of the ingot surface, whereas the thickest step has a role similar to that of the ingot core, transferring heat to the thinner steps.

5. Analysis of the Practical Methods

Predicting fractions of delta ferrite with practical methods consists of two steps: (1) calculating Cr_{eq} and Ni_{eq} using proposed expressions and (2) plotting a point using these indexes as coordinates in a diagram of iso-ferrite lines. The ferrite fraction is obtained from the line that intercepts this point. Some authors[9–12] were only interested in establishing the equivalent effect of several elements in the amount of residual delta ferrite. Therefore, they proposed expressions to calculate Cr_{eq} and Ni_{eq} based on experiments, but did not give any iso-ferrite line diagram. If these indexes were correctly determined, they could be used to plot the points in

an iso-ferrite line diagram obtained by a different author, finally determining the ferrite fraction. Theoretically, these iso-ferrite lines could be obtained using alloy compositions completely different from those used to obtain Cr_{eq} and Ni_{eq}. For example, an iso-ferrite line diagram could be constructed using simple ternary Fe–Cr–Ni alloys and these lines could, in principle, be used in combination with the Cr_{eq} and Ni_{eq} expressions derived by Hull[11] to estimated the ferrite fraction. Consequently, combinations of Cr_{eq} and Ni_{eq} indexes and iso-ferrite line diagrams proposed by different authors were adopted to predict the residual ferrite content in the present work samples.

Nineteen versions of practical methods were defined by a combination of an expression to calculate Cr_{eq} and Ni_{eq} (step 1) and a diagram of iso-ferrite line (step 2). Each method was analyzed by comparing its estimates with the experimental fractions obtained in the present work specimens and those given in the reports presented by the Jernkontoret[13] and by Hull.[11] The ferrite fractions presented by Hull[11] were measured in pins (5.1 cm in length and 0.6 cm in diameter) of 70 types of alloys cast in copper molds. The fractions reported by the Jernkontoret[13] were obtained from samples cooled in a special furnace that imposed cooling rates (0.1 to 2 K/s) typical of those in small and medium size castings.

5.1. Equations Describing the Diagrams of Iso-ferrite Lines

As described before, to predict delta ferrite fractions with practical methods the values of Cr_{eq} and Ni_{eq} calculated for a specific alloy composition should be used to plot a point in a diagram of iso-ferrite lines. The line intercepting this point gives the amount of ferrite. If the point is located in between two iso-ferrite lines, some type of interpolation is necessary. Therefore, the iso-ferrite lines of four important diagrams were represented by equations.

The diagrams of iso-ferrite lines proposed by Schaeffler,[3] DeLong,[5] and Siewert,[7] which were developed for stainless steel welds, and that proposed by Schoefer[14] for castings were described by equations. In the case of Schaeffler[3] diagram, all the iso-ferrite lines plotted in the original diagram were assumed to have a common pivot point and different angular coefficients. To estimate the ferrite fraction for a point located in between these lines, the angular coefficients of the two nearest neighbor lines were used to construct a linear interpolation equation as a function of the ferrite fraction. The final equation to determine the amount of ferrite (*FE*) from the Cr_{eq} and Ni_{eq} indexes is

$$FE\,(\%) = a \cdot \left(\frac{Ni_{eq} + 2}{Cr_{eq} - 5.4} \right) + b \quad \text{..... (6)}$$

where the constants *a* and *b* are given in **Table 5** for different ranges of ferrite fraction.

To derive the interpolation linear equations for the iso-ferrite lines in the DeLong[5] and Siewert[5] diagrams, the coordinates of the two extreme points of each line in the original diagrams were first determined. These coordinates were then used to construct a linear equation of coordinates as a function of the ferrite fraction. Finally, the equation could be used to determined the coordinates of the line that intercepts a point in between. The final equation for the two diagrams is

$$FE\,(\%) = \frac{Ni_{eq} - \left(a_1 + a_2 \cdot Cr_{eq} \right)}{b_1 + b_2 \cdot Cr_{eq}} \quad \text{..... (7)}$$

where a_1, a_2, b_1, and b_2 are constant coefficients given in **Table 6**.

Schoefer[14] did not explicitly propose a diagram of iso-ferrite lines, but these lines can be extracted from Eq. (3). The four iso-ferrite line diagrams constructed from these equations are given in **Fig. 5**. The modifications of the iso-ferrite lines of the Schaeffler[3] diagram proposed by DeLong[5] are evident (Fig. 5(a)): the DeLong[3] lines are shifted counterclockwise, giving larger ferrite fractions in the upper-right region of the diagram. Note that besides modifying the iso-ferrite lines, DeLong[3] also proposed a new formula for Ni_{eq} to include the effects of N. A relatively small modification was later proposed by Siewert,[7] as can be seen in Fig. 5(b).

The iso-ferrite lines implicit in Schoefer's[14] equation (Eq. (3)), however, are significantly different from those in Siewert[7] and DeLong[5] diagrams (Fig. 5(b)). The lines are shifted to the left, giving much higher ferrite fractions for the same Cr_{eq} and Ni_{eq} indexes. The expressions proposed

Table 5. Constant coefficients *a* and *b* used in Eq. (6) to describe the iso-ferrite lines in the Schaeffler diagram for different ranges of ferrite fraction (FE).

a	*b*	FE (vol%)
–55.6	60.6	0–5
–41.7	46.7	5–10
–64.5	66.8	10–20
–190.5	158.1	20–40
–296.3	223.7	40–80
–121.2	138.8	80–100

Table 6. Constant coefficients a_1, a_2, b_1, and b_2 used in Eq. (7) to describe the iso-ferrite lines of the DeLong[5] and Siewert[7] diagrams for different ranges of ferrite fraction (FE).

Author	a_1	b_1	a_2	b_2	FE (vol%)
DeLong	–12.268	–0.3721	1.3949	–0.00388	0–2
	–12.530	–0.2412	1.4027	–0.00778	2–4
	–12.633	–0.2155	1.4020	–0.00761	4–6
	–12.848	–0.1796	1.4122	–0.00930	6–7.6
	–12.892	–0.1738	1.4182	–0.0101	7.6–9.2
	–13.542	–0.1032	1.4472	–0.0132	9.2–10.7
	–13.523	–0.1050	1.4372	–0.0123	10.7–12.3
	–12.782	–0.1652	1.4230	–0.0112	12.3–13.8
Siewert	–9.547	–0.2620	1.2766	–0.0243	0–2
	–9.926	–0.0727	1.2721	–0.0222	2–4
	–10.37	0.0383	1.2500	–0.0167	4–6
	–10.748	0.1014	1.2958	–0.0243	6–7.6
	–8.745	–0.1622	1.1763	–0.00866	7.6–9.2
	–8.0629	–0.2364	1.1523	–0.00597	9.2–10.7
	–10.333	–0.0242	1.2054	–0.0109	10.7–12.3
	–10.920	0.0235	1.2325	–0.0131	12.3–13.8

by Schoefer[14] to calculate Cr_{eq} and Ni_{eq} are also significantly different (see Table 1) from those proposed by the previous authors. As a result, some part of these large differences cancel out and the estimates of ferrite fractions given by Schoefer[14] are not substantially different from those of the previous authors.

5.2. Predictions and Error Analysis

Ferrite fractions calculated with practical methods are compared with three different sets of experimental fractions: (1) measured in the present work, (2) reported by the Jernkontoret,[13] and (3) reported by Hull.[11] Nineteen different versions of practical methods were defined by combining several expressions for the Cr_{eq} and Ni_{eq} indexes with different diagrams of iso-ferrite lines, which finally give an estimate of the ferrite fraction for a certain alloy composition. Schaeffler,[3] DeLong,[5] Siewert,[7] and Schoefer[14] all proposed both a diagram and expressions for the Cr_{eq} and Ni_{eq}. Therefore, these were chosen for the analysis. On the other hand, Schneider,[9] Hull,[11] Hammar and Svensson,[12] Espy,[6] and Guiraldenq[10] suggested expressions for Cr_{eq} and Ni_{eq} (see Eqs. (1) and (2) and Table 1), but did not propose any new diagram of iso-ferrite lines. Consequently, to calculate the ferrite fractions, their expressions were combined with the diagrams suggested by Schaeffler,[3] DeLong,[5] and Siewert.[7] In all, nineteen (= 4 + 3 × 5) different versions of the practical method were used to calculate ferrite fractions for each alloy composition as follows: Cr_{eq} and Ni_{eq} were obtained using Eqs. (1), (2), and the coefficients in Table 1, and the ferrite fractions were finally calculated with Eqs. (3), (6), and (7), and the coefficients in Tables 5 and 6 for each iso-ferrite line diagram. The number of alloys analyzed for each of the nineteen versions of the practical method varied between 37 and 276.

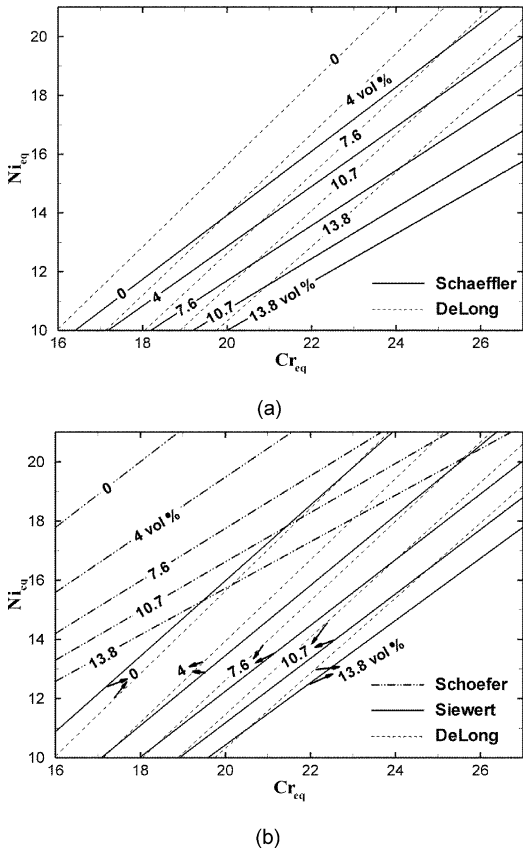

Fig. 5. Diagrams of iso-ferrite lines constructed from the equations given in the present work: (a) Schaeffler[3] and DeLong;[5] (b) Siewert,[7] Schoefer,[14] and DeLong.[5]

As shown in Table 1, four of the Cr_{eq} and Ni_{eq} indexes adopted to define a practical method were developed from studies in weld samples, but are applied to the cast samples analyzed in the present work. Generally, the larger cooling rates in weld samples could result in different ferrite amounts from those in the present cast samples. However, the results presented in section and those published in the literature have usually shown a weak effect of cooling rate on the amount of residual ferrite. In the samples reported by the Jernkontoret[13] (Fig. 3), for example, no clear trend is observed in the cooling rate range between 0.1 and 2 K/s. Pereira and Beech[23] observed variations of ferrite fractions from approximately 5 to 8 vol% after increasing the cooling rate from 0.42 to 32 K/s for steels in solidification mode FA. Kim *et al.*[25] noticed a change in the fraction of ferrite from 4 to 8 vol% along the cross section of a plate. Therefore, owing to the relatively weak effect of cooling rate, indexes and iso-ferrite lines carefully developed from weld samples were also used to define some of the practical methods used in the present work to predict ferrite quantity in cast samples.

In the comparisons between calculated and measured ferrite fractions, two groups of alloys were created: one group with composition in the restricted range given in **Table 7** and another group in the extended range. The restricted range defines a group that approximately fulfills all composition ranges of the alloys employed to derive the Cr_{eq} and Ni_{eq} expressions and diagrams used in the present analysis. The extended range, on the other hand, obviously yielded a larger group of alloys and was defined to show the behavior of the practical methods outside of the composition range in which they were developed. Basically, most of the measurements presented by Hull[11] were not included in the restricted range group, because the alloys belong to a much broader range of compositions. All the alloys with measured ferrite fractions larger than 13.8 vol% were removed from the study, because this is the limit in DeLong[5] diagram. In each calculation, when the values of Cr_{eq} and Ni_{eq} for a given alloy composition were out of the range for the diagram of iso-ferrite lines, the corresponding alloy was also removed from the analysis.

In **Fig. 6**, calculations of delta ferrite fractions using the nineteen versions of the practical methods applied to the

Table 7. Restricted and extended composition ranges of element concentrations (mass%) used to define two groups of alloys.

	C	Mn	Si	Cr	Ni	Mo	Cu	Nb	N	Al	Ti	W	V	Co
Rest	< 0.1	< 1.85	< 1.3	16–24	9–14	< 3	< 0.25	< 0.8	< 0.1	< 0.08	< 0.008	< 0.04	< 0.08	< 0.1
Ext	< 0.3	< 20	< 4	12–32	4–25	< 6	< 4	< 4	< 0.2	< 2	< 2	< 5	< 4	< 6

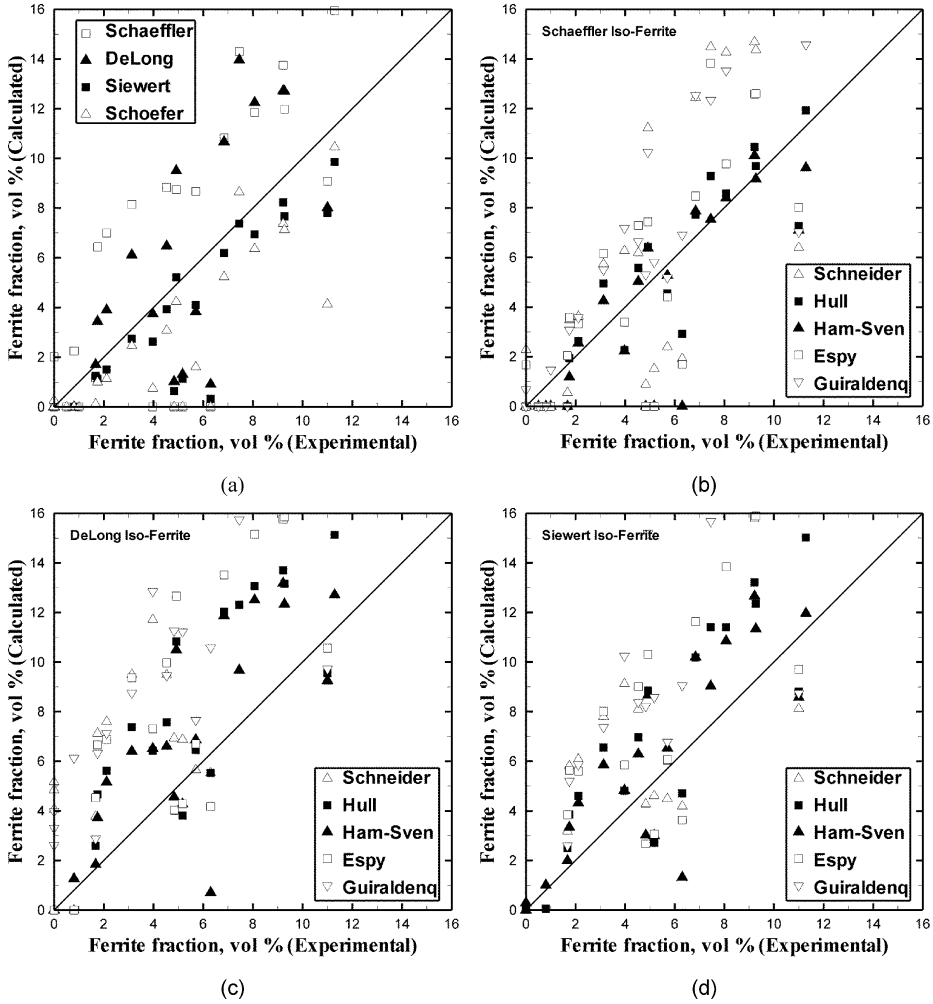

Fig. 6. Calculated versus measured delta ferrite fractions for the alloys in the extended composition range, after eliminating measurements by Hull.[11] Fractions were calculated using: (a) Cr_{eq}, Ni_{eq}, and iso-ferrite lines proposed by Schaeffler,[3] DeLong,[5] Siewert *et al.*,[7] and Schoefer;[14,15] (b) iso-ferrite lines proposed by Schaeffler,[3] (c) DeLong,[5] and (d) Siewert *et al.*,[7] using Cr_{eq}, Ni_{eq} defined by Schneider,[9] Hull,[11] Hammar and Svensson,[12] Espy,[6] and Guiraldenq.[10]

alloys in the extended composition range are given as a function of the measured fractions. In this figure, the calculations for the alloys presented by Hull[11] were not included, because they increase the number of points substantially, preventing the visualization of any trend in the data. Figure 6(a) gives the calculations using the four practical methods in which both the expressions for Cr_{eq}, Ni_{eq} and the iso-ferrite line diagram were given by the same author, whereas Figs. 6(b), 6(c), and 6(d) show separately the calculations using one iso-ferrite line diagram and several expressions for Cr_{eq} and Ni_{eq}. To help interpret the results, some statistical parameters were calculated for each group of alloy as follows

$$\text{relative error (\%)} = \sum_{i=1}^{N}\left\{\frac{\left|FE_{exp,i} - FE_{calc,i}\right|}{N \cdot FE_{exp,i}}\right\} \quad \text{.....(8)}$$

$$\text{error} = \frac{\sum_{i=1}^{N}\left(FE_{exp,i} - FE_{calc,i}\right)}{N} \quad \text{.....(9)}$$

$$\text{SD} = \sqrt{\frac{\sum_{i=1}^{N}\left[\left(FE_{exp,i} - FE_{calc,i}\right) - error\right]^2}{N-1}} \quad \text{.....(10)}$$

$$\text{CI} = \pm t_{\frac{0.05}{2},N-1}\frac{SD}{\sqrt{N}} \quad \text{.....(11)}$$

where $FE_{exp,i}$ and $FE_{calc,i}$ are respectively the measured and calculated ferrite fractions in sample i of a group with N samples, *i.e.*, N alloys; error is the average of the errors between calculated and measured ferrite fractions in the group; relative error is the average of the relative errors (measured fractions equal to zero were not included); SD is the standard deviation of the errors; CI is the critical interval to assume, with 5% of significance level ($\alpha = 0.05$), that the average *error* given by Eq. (9) comes from a population with zero average error; and $t_{0.05/2,\ N-1}$ is the value of a t-Student distribution with N-1 degrees of freedom and significance level of $\alpha = 0.05$.

Using the parameters in Eqs. (8) to (11), three types of errors were analyzed for each practical method: (1) a combination of systematic and random errors, given by the absolute relative error in Eq. (8), which reveals the general quality of the method; (2) systematic errors, which are related to the existence of bias[7] and are calculated with Eq. (9), in which random positive and negative errors cancel out; and (3) random errors, showing the dispersion in the calculations, given by SD in Eq. (10). During the development of

a practical method, it becomes biased if important variables (*e.g.*, specific chemical elements, processing conditions) that have an effect always in the same direction (*i.e.*, always either increase or decrease the ferrite fractions) are neglected. The method was considered biased when the average error (Eq. (9)) was outside of the critical interval given by CI (Eq. (11)). Larger SD values suggest that important variables that have random effects on the ferrite fractions were not considered during development of the practical method. Note that the average relative error (Eq. (8)) indicates the combined effects of systematic and random errors and tend to be low when these errors are low.

The four parameters given by Eqs. (8) to (11) are shown in **Tables 8** and **9** for each of the nineteen versions of the practical methods applied to the alloys in the restricted and extended composition range, respectively. There are four sets of rows in each table and, for Table 9, each set corresponds to one graph of Fig. 6. Within a set, each individual row gives the statistical parameters for one set of points in the graph. For example, the second row within the third set in Table 9 gives the statistical parameters for the set of black squares in Fig. 6(c), which were obtained using the expressions for the Cr_{eq}, Ni_{eq} proposed by Hull[11] and the iso-ferrite line diagram proposed by DeLong.[5]

Important conclusions valid for the two groups of alloys can be obtained from Tables 8 and 9. The most important one is that calculations with Siewert diagram (Siew/Siew) give the smallest relative errors (≈ 43% and 58% for the restricted and extended composition ranges, respectively), followed by the combination of Hull expressions for Cr_{eq} and Ni_{eq} and Schaeffler iso-ferrite lines (Hull/Scha), and Hammar and Svensson expressions combined with Siewert iso-ferrite lines (Ham-Sve/Siew). This conclusion cannot be drawn from visual examination of Fig. 6, showing the importance of the statistical analysis. These lowest relative errors are a consequence of a good combination of low random and systematic errors, which are shown, respectively, in the SD and Error columns in Tables 8 and 9. The good quality of the practical methods that use Siewert diagram or Hull expressions for Cr_{eq} and Ni_{eq} indexes should not be a surprise, since a very large number of alloy compositions were considered in their analysis.

The separate effect of each expression to calculate Cr_{eq} and Ni_{eq} on the relative error can be analyzed by comparing the table rows obtained with the same diagram of iso-ferrite lines. Therefore, each row should be compared only with rows belonging to the same set. For the 2nd, 3rd, and 4th sets of rows in both tables, the expressions proposed by Hull[11] and Hammar and Svensson[12] give the lowest relative error. As expected, they also have the lowest systematic and random errors (SD and Error columns). This aspect can be seen in Figs. 6(b), 6(c), and 6(d), showing that the two sets of black symbols are generally closer to the diagonal line than the sets of open symbols.

The relative errors in Tables 8 and 9 clearly confirm that the Siewert diagram is an improvement on the diagrams pro-

Table 8. Relative error, error, standard deviation (SD) and the critical error interval (CI) for a group of N alloys in the restricted composition range. The abbreviations are: Scha (Schaeffler[3]); DL (DeLong[5]); Siew (Siewert[7]); Scho (Schoefer[14]); Schn (Schneider[9]); Hull[11]; Ham-Sve (Hammar and Svensson[12]); Espy[6]; and Guir (Guiraldenq[10]).

Cr_{eq},Ni_{eq}/Iso-ferrite line	Rel Error(%)	Error	SD	CI	N
Scha/Scha	66	–0.01	3.18	± 0.93	47
DL /DL	75	1.10	3.21	± 0.99	43
Siew/Siew	43	–0.18	2.38	± 0.74	42
Scho/Scho	52	–1.69	2.39	± 0.70	47
Schn/Scha	70	0.68	3.74	± 1.10	47
Hull/Scha	46	–0.42	2.40	± 0.70	47
Ham-Sve/Scha	50	–0.87	2.39	± 0.70	47
Espy/Scha	69	0.72	3.34	± 0.98	47
Guir/Scha	90	2.71	4.67	± 1.37	47
Schn/DL	126	3.78	4.82	± 1.48	43
Hull/DL	77	1.70	2.90	± 0.90	42
Ham-Sve/DL	66	1.46	2.55	± 0.80	42
Espy/DL	122	3.38	3.71	± 1.24	37
Guir/DL	167	5.85	4.50	± 1.50	37
Schn/Siew	100	3.41	4.57	± 1.42	42
Hull/Siew	58	1.39	2.71	± 0.84	42
Ham-Sve/Siew	48	1.25	2.28	± 0.71	42
Espy/Siew	97	2.80	3.80	± 1.20	41
Guir/Siew	137	5.51	4.77	± 1.50	41

Table 9. Relative error, error, standard deviation (SD) and the critical error interval (CI) for a group of N alloys in the extended composition range. The abbreviations are: Scha (Schaeffler[3]); DL (DeLong[5]); Siew (Siewert[7]); Scho (Schoefer[14]); Schn (Schneider[9]); Hull[11]; Ham-Sve (Hammar and Svensson[12]); Espy[6]; and Guir (Guiraldenq[10]).

Cr_{eq},Ni_{eq}/ Iso-ferrite line	Rel Error (%)	Error	SD	CI	N	Fig.
Scha/Scha	83	–1.85	3.99	± 0.47	276	6(a)
DL/DL	89	–1.18	4.34	± 0.57	224	
Siew/Siew	58	0.10	3.22	± 0.54	138	
Scho/Scho	76	–2.33	3.61	± 0.44	267	
Schn/Scha	135	2.33	7.88	± 0.93	276	6(b)
Hull/Scha	62	0.98	4.66	± 0.55	276	
Ham-Sve/Scha	77	–1.95	3.54	± 0.42	276	
Espy/Scha	167	5.50	11.52	± 1.37	276	
Guir/Scha	116	1.41	6.65	± 0.79	276	
Schn/DL	170	3.79	7.53	± 0.99	223	6(c)
Hull/DL	96	2.46	3.33	± 0.45	215	
Ham-Sve/DL	89	–1.16	4.17	± 0.55	221	
Espy/DL	165	4.41	6.14	± 0.91	179	
Guir/DL	152	2.87	6.30	± 0.86	208	
Schn/Siew	169	5.40	7.44	± 1.09	180	6(d)
Hull/Siew	70	2.37	2.98	± 0.42	195	
Ham-Sve/Siew	67	0.14	3.82	± 0.65	134	
Espy/Siew	156	5.43	6.22	± 0.98	156	
Guir/Siew	156	5.05	6.30	± 1.00	155	

posed by Schaeffler[3] and DeLong,[5] as intended by its author. This can also be seen in Fig. 6(a), in which calculations for the Schaeffler and DeLong diagrams are farther from the diagonal line. These larger errors for the Schaeffler diagram cannot be attributed to the differences in cooling rates between weld samples (used to construct Schaeffler diagram) and the cast samples used in the present analysis, since the Siewert diagram was also developed for welds. Although Siewert diagram was constructed for weld samples, its calculations for the cast samples examined in the present work gave errors lower than those methods specially developed for castings, *i.e.*, Schoefer's method[14] and combinations of Cr_{eq} and Ni_{eq} given by Schneider[9] and Guiraldenq.[10] This suggests that the difference between cooling rates experienced by weld and cast samples may not significantly change the amount of residual ferrite observed at room temperature, which agrees with the results presented in Section 4 for the weak effect of cooling rate.

On the other hand, a simple examination of Figs. 6(c) and 6(d) could give the impression that a clear trend exists of a decrease in the ferrite fraction with a decrease in the cooling rate. In these figures, most of the experimentally measured fractions (for castings) are lower than the calculated fractions, obtained from iso-ferrite lines developed for weld samples, in which the cooling rates are much higher. Nevertheless, Fig. 6(a) shows an opposite trend, *i.e.*, measured fractions are higher than most of the fractions calculated with Siewert diagram and higher than approximately half of the fractions calculated with DeLong diagrams. Both these diagrams were developed from weld samples, in which the cooling rate is higher than that in cast samples, indicating an increase in ferrite fraction with a decrease in cooling rate. The opposite trend observed in these figures might also suggest a weak effect of the cooling rate, easily outweighed by other effects and preventing a clear tendency from being revealed.

Special attention should be given to the Schoefer's method,[14] because it is currently an ASTM standard procedure to estimate delta ferrite fractions in stainless steel castings.[15] Although this method showed relative errors that are larger than those for the Siewert diagram, its errors are lower than those obtained with most of the nineteen practical methods examined in the present work. The individual errors obtained with Siewert diagram and with Schoefer's method[14] are shown in detail in **Fig. 7**.

The discussion presented in the previous paragraphs is valid for the alloys in both the restricted and extended composition ranges and, consequently, is not affected by composition. There are some conclusions, however, that are valid only for either group, showing the effect of composition. For the alloys in the restricted composition range, Table 8 shows that a combination of Schaeffler iso-ferrite lines and different expressions for Cr_{eq} and Ni_{eq} (2nd set of rows) gives the lowest relative errors when compared with calculations using either DeLong or Siewert iso-ferrite lines with the same expressions for Cr_{eq} and Ni_{eq}. This is concluded by comparing the rows for the same Cr_{eq} and Ni_{eq} expressions in different sets of rows. Note that the 2nd set of rows has lower random (SD column) and systematic (Error column) errors than the 3rd and 4th sets of rows. Particularly the systematic errors for Schaeffler iso-ferrite lines are much lower than those for DeLong and Siewert iso-ferrite lines. In the 1st set of rows, it can be seen that the systematic error for the Schaeffler diagram is also the lowest among all four methods examined. This suggests that the improvements proposed by Siewert[7] were largely due to a reduction in random errors, accomplished mainly by defining different expressions for Cr_{eq} and Ni_{eq}.

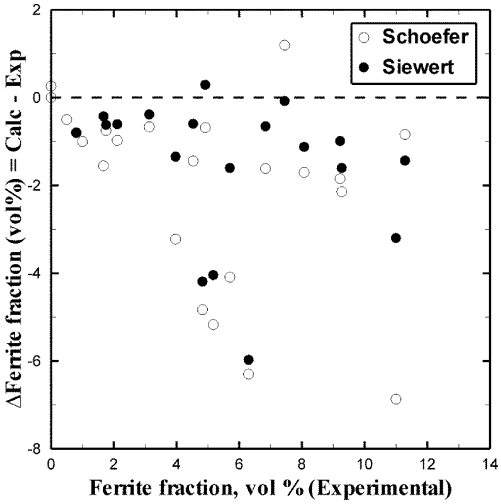

Fig. 7. Error for individual calculations of ferrite fractions using Siewert diagram[7] and Schoefer method[14] for the alloys in the extended composition range, after eliminating measurements by Hull.[11]

When the practical methods are applied to a broader range of alloy composition (Table 9), the errors arising from Schaeffler iso-ferrite lines are larger. The practical methods using Schaeffler iso-ferrite lines (2nd set of rows in Table 9) give the largest random errors (SD column). This was expected, because the group of extended composition range includes alloys with element concentrations very different from those used to construct Schaeffler diagram. Actually, a comparison between Tables 8 and 9 shows that the relative errors for the extended composition range are larger in eighteen of the nineteen methods examined and that this is owing to a major increase in the random errors (SD column), rather than in the systematic errors (Error column).

The Error column in Tables 8 and 9 may indicate the amount of bias in each practical method. To elaborate a more accurate conclusion, however, the hypothesis test described earlier was carried out by verifying whether the values in the Error column were within the critical interval defined in the CI column. This analysis suggests that five practical methods are unbiased for the alloys in the restricted composition range (Table 8), four of them derived from Schaeffler iso-ferrite lines, but only two methods are unbiased for the alloys in the extended range (Table 9). The large concentrations of some elements in some of the alloys in the extended composition range were not considered in the development of most of the practical methods, resulting in undesired bias.

6. Summary and Conclusions

Measurements of delta ferrite carried out in the present work and by the Jernkontoret[13] and Hull[11] were used to evaluate nineteen different versions of practical methods

(nickel/chromium equivalent indexes and iso-ferrite line diagrams) to estimate residual ferrite fractions in austenitic stainless steel castings. Designed with different step thicknesses, ladder shaped specimens cast in the present work showed the effects of cooling rate on the amount of residual ferrite in the microstructure.

In the ladder shaped samples, a change in cooling rate from 0.78 to 2.7 K/s has a weak effect on the amount of delta ferrite. In approximately 50% of the specimens with ferrite in their microstructures, a hypothesis test indicates that an increasing cooling rate decreases the amount of delta ferrite, in agreement with some results presented by Kim *et al*.[25] and Pereira and Beech.[23] In the remaining specimens, no effect was detected. Optical microscopy showed that, for ferrite fractions over 10 vol%, there is an almost continuous ferrite network, whereas for ferrite fractions of about 5 vol%, the network becomes semi-continuous, changing to isolated cores for fractions lower than approximately 2 vol%.

Calculations of ferrite fractions using the practical method proposed by Siewert[7] give the lowest relative error among all the nineteen methods examined in the present work. Low relative errors were also obtained by two practical methods using the following combination: (a) nickel/chromium equivalent indexes proposed by Hull[11] with iso-ferrite lines suggested by Schaeffler[3] and (b) nickel/chromium equivalent indexes proposed by Hammar and Svensson[12] with iso-ferrite lines suggested by Siewert.[7] These three practical methods give a good combination of low systematic and random errors. Although the Siewert diagram was constructed for stainless steel welds, estimates of ferrite fractions using this diagram in cast samples are more accurate than those calculated with the method of Schoefer,[14] specially developed for cast samples and currently adopted as an ASTM standard[15] to predict residual ferrite fractions in stainless steels castings.

When combined with any of the three diagrams of iso-ferrite lines proposed by Schaeffler,[3] DeLong,[5] or Siewert,[7] the expressions derived by Hull[11] or by Hammar and Svensson[12] to calculate the nickel and chromium equivalent indexes give the lowest relative error among all other equivalent index expressions. On the other hand, for alloys in a restricted composition range, expressions of nickel and chromium equivalents give the lowest relative errors when combined with Schaeffler iso-ferrite lines. When alloys with a broader composition range are included in the analysis, the relative errors increase in eighteen of the nineteen practical methods examined as a result of an increase in random errors.

Acknowledgements

The authors wish to thank FAPESP (Fundação de Amparo à Pesquisa do Estado de São Paulo) for the financial support to this work (grants 95/9113-2, 96/04242-1, and 03/08576-7) and Açotécnica SA for providing the samples.

REFERENCES

1) A. F. Padilha and P. R. Rios: *ISIJ Int.*, **42** (2002), 325.
2) D. L. Olson: *Weld. J.*, **64** (1985), S281.
3) A. L. Schaeffler: *Met. Prog.*, **56** (1949), 680.
4) S. Fukumoto, K. Fujiwara, S. Toji and A. Yamamoto: *Mater. Sci. Eng. A*, **492** (2008), 243.
5) W. T. DeLong: *Met. Prog.*, **77** (1960), 98.
6) R. H. Espy: *Weld. J.*, **61** (1982), S149.
7) T. A. Siewert, C. N. McCowan and D. L. Olson: *Weld. J.*, **67** (1988), S289.
8) D. J. Kotecki and T. A. Siewert: *Weld. J.*, **71** (1992), S171.
9) H. Schneider: *Foundry Trade J.*, **108** (1960), 562.
10) P. Guiraldenq: *Mem. Sci. Rev. Met.*, **64** (1967), 907.
11) F. C. Hull: *Weld. J.*, **52** (1973), 193.
12) Ö. Hammar and U. Svensson: Solidification and Casting of Metals, The Metals Society, London, (1977), 401.
13) Jernkontoret: A Guide to the Solidification of Steels, Jernkontoret, Stockholm, (1977).
14) E. A. Schoefer: *Metal Progress Databook*, **112** (1977), 51.
15) ASTM Standard Practice for Steel Casting, Austenitic Alloy, Estimating Ferrite Content Thereof (800/A 800M-01). Steel, Stainless Steel, and Related Alloys. ASTM International, West Conshohocken, Philadelphia, PA, (2006). 1.
16) Y.-H. Park and Z.-H. Lee: *Mater. Sci. Eng. A*, **297** (2001), 78.
17) P. L. Ferrandini, C. T. Rios, A. T. Dutra, M. A. Jaime, P. R. Mei and R. Caram: *Mater. Sci. Eng. A*, **435** (2006), 139.
18) A. Di Schino, M. G. Mecozzi, M. Barteri and J. M. Kenny: *J. Mater. Sci.*, **35** (2000), 375.
19) D. C. Montgomery and G. C. Runger: Applied Statistics and Probability for Engineers, Wiley, Hoboken, NJ, (2007).
20) T. Yamada, S. Okano and H. Kuwano: *J. Nucl. Mater.*, **350** (2006), 47.
21) G. El Nayal and J. Beech: *Mater. Sci. Technol.*, **2** (1986), 603.
22) N. Suutala and T. Moisio: Solidification Technology in the Foundry and Cast House, The Metals Society, London, (1980), 310.
23) O. J. Pereira and J. Beech: Solidification Technology in the Foundry and Cast House, The Metals Society, London, (1980), 315.
24) J. W. Elmer, S. M. Allen and T. W. Eagar: Recent Trends in Welding Science and Technology - TWR '89, ASM International, Materials Park, Ohio, (1989), 169.
25) S. K. Kim, Y. K. Shin and N. J. Kim: *Ironmaking Steelmaking*, **22** (1995), 316.
26) H. D. Brody and M. C. Flemings: *Trans. Met. Soc. AIME*, **236** (1966), 615.
27) M. C. Flemings: Solidification processing, McGraw-Hill, New York, (1974).
28) M. A. Martorano and J. D. T. Capocchi: *Metall. Mater. Trans. A*, **31** (2000), 3137.